A Dynamically Responsive Surface with Switchable Wettability for Efficient Evaporation and Self-cleaning Abilities

Gregory Parisi, Alejandro Lopez, Shankar Narayan*
Department of Mechanical, Aerospace, and Nuclear Engineering.
Rensselaer Polytechnic Institute, 110 8th Street, Troy, NY 12180.
* Corresponding Author: narays5@rpi.edu

Abstract

Evaporation is crucial in many applications. One of the critical parameters affecting evaporation is surface wettability, which is often tailored using coatings and micro or nanoscale features on the surface. While this approach has advanced many technologies, the ability to control wettability dynamically can add new functionalities and capabilities that were not possible before. This study demonstrates how a self-cleaning superhydrophobic surface with an equilibrium contact angle of 155^o can dynamically change to a superhydrophilic surface with a contact angle near 0^o, resulting in drastically different evaporation characteristics. Specifically, we find that the evaporation rate and surface temperature reduction due to the resulting cooling are 3-times higher due to the change in surface wettability. This change in wetting behavior is due to the use of an amino-silane (N-(2-Aminoethyl)-11-aminoundecyltrimethoxysilane)-functionalized surface, which is altered in the presence of dilute acetic acid. Upon complete evaporation, the surface reverts to superhydrophobic behavior. This reversible behavior is not seen in traditional non-wetting coatings like perfluorodecyltrichlorosilane and lauric acid. This strategy for dynamic control of wettability and evaporation can lead to advancements in many applications ranging from self-assembly-based fabrication processes to oil-water separation and advanced thermal management technologies.

Keywords

Switchable Wettability; Dynamic Wettability; Dynamic Contact Angle: Switchable Evaporator; Dynamic Evaporator; Self-cleaning Surface; Thin-film Evaporation; Evaporative Cooling

Introduction

Droplet evaporation is essential in many applications, including lab-on-a-chip technologies[1], inkjet printing[2–4], biosensing[5], manufacturing[6], and cooling[7–10]. Evaporation is strongly coupled to the wettability of a surface, as observed in several studies. For example, biphilic patterns consisting of hydrophilic and hydrophobic spots are known to affect droplet evaporation[11,12] and boiling characteristics of water[13]. Wettability can affect the crystalline patterns resulting from the evaporation of saline droplets[14], the efficacy of transparent heaters for deicing surfaces[15], solar-water desalination[16], a quartz crystal microbalance's response to droplet evaporation[17], and the self-assembly of particles in nanofabrication[18]. Likewise, droplets evaporating on chemically patterned surfaces could become unstable and break up due to different surface wettabilities[19]. Besides, extreme wetting or non-wetting surfaces are often desired for self-cleaning[20], anti-fogging[21], anti-icing[22], and antibacterial action[23,24], where the substrate is modified with coatings and micro and nanoscale roughness.

Improving evaporation kinetics using thin liquid films requires super-wetting surfaces, while vapor-to-liquid dropwise condensation and self-cleaning surfaces favor non-wetting characteristics[25–27]. A spherical or non-wetting evaporating droplet has to rely on heat diffusion across the drop[28], which can be inefficient, resulting in slow evaporation kinetics. Strategies to overcome this limitation include preheating the evaporating liquid, which can reduce the time to heat a relatively cold droplet and the total evaporation time[29]. Recent efforts for improvement include the use of microgrooved surfaces on polished silicon, which enhances droplet spreading and lowers evaporation time[30]. Likewise, fabrics allowing water to spread and evaporate quickly can be eco-friendly low-energy alternatives for air-conditioning[31].

Although several studies have shown cooling rate enhancement with permanent changes in surface wettability, using a dynamically switchable surface is relatively uncommon[32–35]. While tailoring wetting properties has benefited many applications, the ability to switch wettability dynamically can allow additional functionalities and capabilities. Dynamic surfaces can transition between superhydrophobic and superhydrophilic states, often with an external stimulus. Such surfaces have broad applications in controllable drug release[36], oil-water separation[37–39], and condensation[40].

The significance of the present study is the demonstration of both self-cleaning and thin-film evaporative cooling characteristics. It presents a superhydrophobic surface on which water droplets roll off easily to self-clean the surface. However, the droplets evaporate relatively slowly - by using a slightly modified working fluid, the surface can drastically alter its wettability to a superhydrophilic state. Consequently, the evaporation characteristics change dramatically, yielding a relatively high evaporation rate and surface cooling. This switchability can be helpful in several applications, including filters for oil-in-water and water-in-oil emulsion separation, accelerated self-assembly-based fabrication processes, and advanced active thermal management technologies. Such materials can also reduce the cost of creating multiple surfaces with different wettabilities. Cost savings are also expected from utilizing the same surface for high heat dissipation and self-cleaning, as opposed to using additional resources for cleaning.

Experimental Setup and Procedure

Materials

This study used the following chemicals and materials. N-(2-Aminoethyl)-11-aminoundecyltrimethoxysilane or "amino-silane" ($C_{16}H_{38}N_2O_3Si$) from Gelest, lauric acid (C12H24O2, 99%) from Sigma Aldrich, perfluorodecyltrichlorosilane or FDTS (C10H4Cl3F17Si, 97%) and aluminum foil (0.25 mm thickness, 99% pure) from Alfa Aesar, ethanol (C_2H_5OH, 200 proof) from Thomas Scientific, sodium hydroxide (NaOH, 98.9%) and hydrochloric acid (HCl, 38.0%) from Fisher Chemicals, acetic acid (CH_3COOH, 99.7%,) from Acros Organics and acetone ($(CH_3)_2CO$) from Rensselaer Polytechnic Institute.

Surface Characterization

The surface roughness of aluminum samples was observed using a scanning electron microscope (SEM, Carl Zeiss Supra 55 FESEM), and elemental analysis was performed using energy dispersion spectroscopy (EDS, Oxford Aztec). A digital single-lens reflex camera (Nikon D610)

was used for photos and videos. A contact angle measuring instrument (Rame-Hart, Model 590) was used to characterize wetting behavior and quantify evaporation kinetics. The average contact angles reported in this study are an average of 3 measurements on the same sample, which are provided in the supporting information. Elemental composition was measured using x-ray photoelectron spectroscopy or XPS (PHI 5000 Versaprobe).

Surface Preparation

Flat aluminum foils (1×1 cm) were cleaned ultrasonically in acetone, ethanol, and de-ionized (DI) water for 5 minutes each. The samples were then submerged in a 3% NaOH solution at 90°C for 3 minutes with continuous stirring at 250 RPM. Then the samples were etched in 3M HCl solution for 4 minutes with stirring at 250 RPM. Then the samples were rinsed with DI water and dried with nitrogen gas. The etched aluminum foils were then treated with different surface modification solutions, as shown in Table 1. Finally, the fabricated samples were cleaned in ethanol and placed in an oven (100°C) for 25 minutes to dry.

Table 1. Chemical composition and duration of coatings to prepare hydrophobic samples

Chemicals	Composition	Time (min)
Amino-Silane, Ethanol, DI Water	1%, 98%, 1% (v/v)	5
Lauric Acid, Ethanol	20%, 80% (w/v)	30
FDTS, Ethanol, DI Water	1%, 98.5%, 0.5% (v/v)	5

Experiment Setup

Figure 1 illustrates the closed environmental chamber used to study droplet evaporation. Droplets (~10 µL) containing DI water and 5% acetic acid (v/v) were deposited on the surface through a removable rubber gasket. The goniometer measured the gradual change in droplet volume and contact angle at either 0.2 or 5 FPS (frames per second). The experiments were performed at room temperature (24°C), 1 atm pressure, and slightly varying relative humidity. The aluminum samples were interfaced to a 1×1 cm ceramic (aluminum nitride) heater (Watlow)[41] using a silicone thermal paste (S606C, T-Global Technology) with a nominal thermal conductivity of 5 W/mK[42]. The K-type thermocouple built into the ceramic heater was used for recording the temperature. All experiments were initiated at ~60°C.

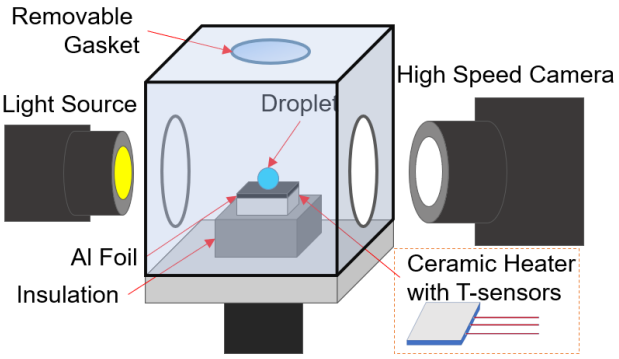

Figure 1. Experimental setup for the evaporation process

The goniometer's profiler quantifies droplet shape and volume, thus allowing calculation of the evaporation rate as a function of time. However, this approach becomes exceedingly challenging when the surface is superwetting since it is difficult to resolve the boundary of the droplet. Hence, another strategy to predict the evaporation rate in this study involved calorimetry - using the change in the temperature of the ceramic heater versus time. Using energy conservation and lumped analysis for an evaporating droplet on the ceramic heater, the equation governing droplet mass (m_d) and evaporation rate ($\dot{m}_d$) is given by:

$$VI - \dot{m}_d h_{fg} - q_h - q_d = m_d c_d \frac{d\theta_d}{dt} + m_h c_h \frac{d\theta_h}{dt} \quad (1)$$

Here, $\theta_d = T_d - T_\infty$ and $\theta_h = T_h - T_\infty$ denote the average droplet and heater temperatures relative to the ambient temperature. q_h and q_d denote heat loss from the surfaces of the heater and droplet to the ambient, respectively. h_{fg} denotes the latent heat of vaporization, and $m_d c_d$ and $m_h c_h$ are the heat capacities of the droplet and the ceramic heater, respectively. V and I are the potential and current flow across the heater.

Infrared imaging of the droplet and heater (supplementary information) indicates that they are in thermal equilibrium ($\theta_d \approx \theta_h$) within a few seconds (~7 s) of droplet deposition. Hence, it is possible to simplify Eqn. (1) by noting that $m_h c_h \gg m_d c_d$ and $q_h \gg q_d$ since the heat capacity and surface areas associated with the ceramic heater are much larger than the droplet (see supplementary information). The following equation allows for calculating the evaporation rate ($\dot{m}_d$) from temperature measurements.

$$\dot{m}_d = \frac{1}{h_{fg}}\left(VI - m_h c_h \frac{d\theta_h}{dt} - q_h\right) \quad (2)$$

For calculating $\dot{m}_d$ at any instant, q_h is calculated by adding the heat loss from each face (A_i) of the ceramic heater as $q_h = \sum_i h_i A_i \theta_h$, which takes into account the orientations of these faces for the calculation of the respective heat transfer coefficients, h_i. The results compare the evaporation rates calculated using Eqn. (2) and the goniometer, showing good agreement indicating that Eqn. (2) is relatively accurate in calculating the dynamic change in evaporation rate. This added capability is handy when quantifying the evaporation rate using visualization becomes challenging. The manuscript will henceforth use water to refer to DI water and acetic acid to imply a 5% acetic acid (v/v) solution to be concise.

Results

Sample Morphology and Composition

SEM images (Figure 2) show that pristine aluminum samples are relatively smooth compared to the aluminum samples after the etching process. Etching creates microstructures on the aluminum substrate, creating air voids throughout the sample. Also, functionalizing the rough surface with a thin chemical layer does not significantly impact the surface morphology. Additional chemical characterizations (EDS), provided in the supplementary data, show successful conformal coating of samples with amino-silane, lauric acid, and FDTS.

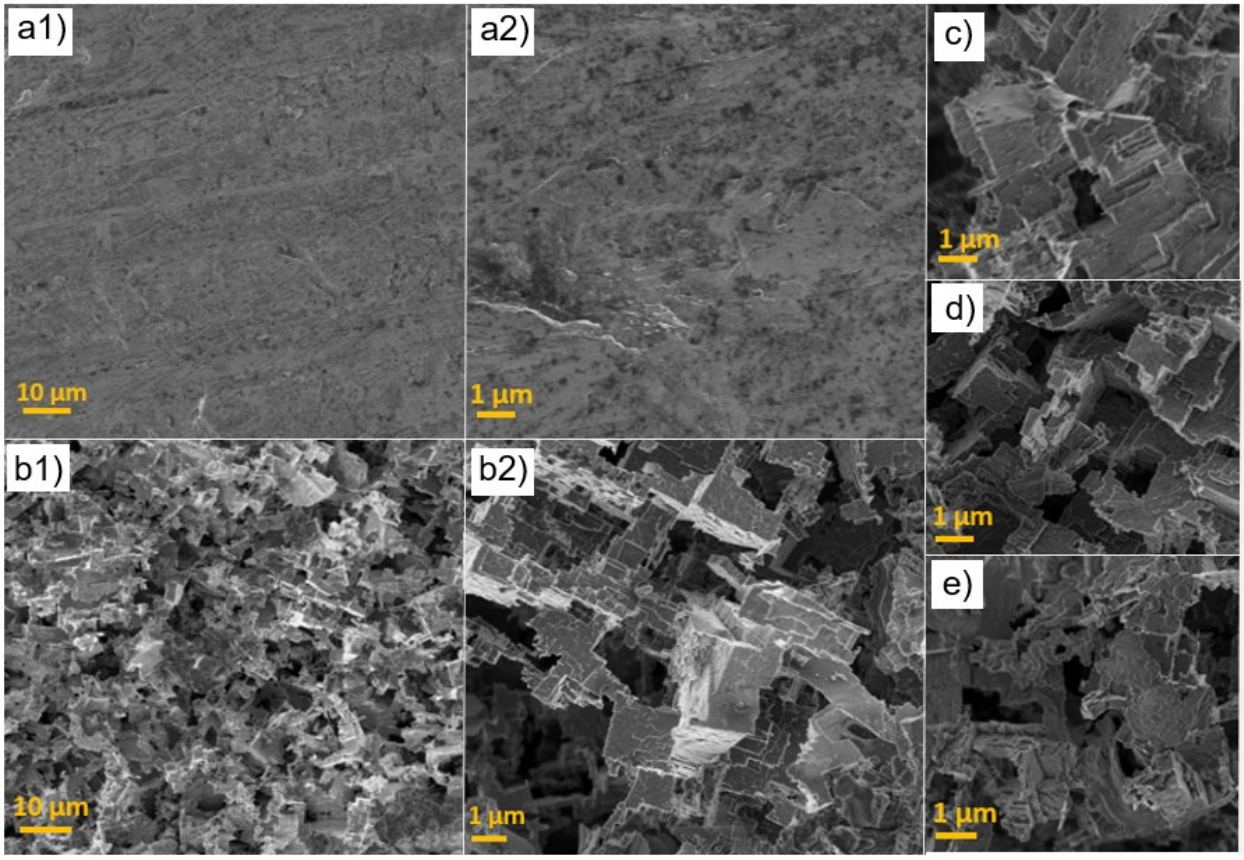

Figure 2. SEM images of the aluminum surface used for evaporation. (a1, a2) Pristine aluminum samples. (b1, b2) Etched aluminum samples. (c) Etched sample after amino-silane modification. (d) Etched sample after lauric acid modification. (e) Etched sample after FDTS modification.

Surface Wettability and Self-Cleaning

The focus of this paper is to create dynamically responsive surfaces for high evaporation rates that also have superhydrophobic self-cleaning capabilities. The amino-silane-modified sample has non-wetting characteristics comparable to frequently used chemicals like lauric acid and FDTS. However, the amino-silane-modified sample can switch to a wetting surface with the addition of acetic acid. The samples coated with FDTS, lauric acid, and amino-silane are shown in Figure 3, with their respective interactions with water and acetic acid. The average contact angles for water on all samples exceed 150°. Although acetic acid drops are non-wetting on FDTS and lauric acid-coated samples, they wet the amino-silane-coated sample. The amino-silane-coated samples show resilience to a wide range of other liquids. Besides studying the non-wetting properties of water, other solutions, including common household liquids, were tested on the amino-silane-coated samples (Figure 4). All liquids, including acidic (HCl) and basic (NaOH) solutions, show non-wetting interactions with the amino-silane-modified surfaces, varying in contact angle based on each liquid's chemistry and surface tension.

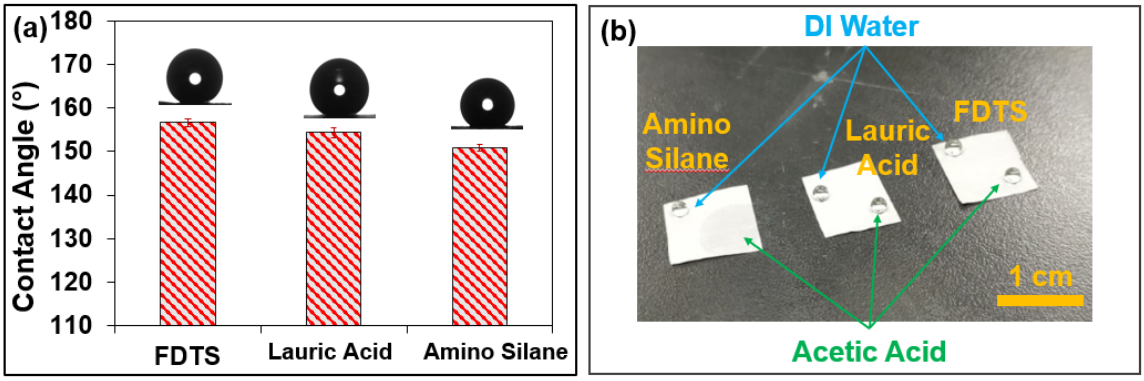

Figure 3. (a) The average contact angle of water on aluminum samples with different coatings. (b) The interaction of water and acetic acid with aluminum samples with different coatings.

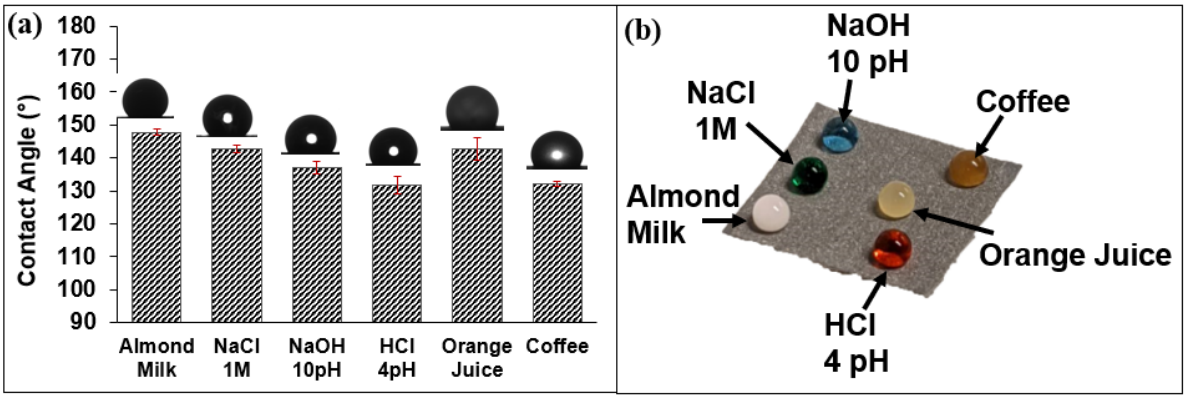

Figure 4. (a) Contact angle measurements of different household liquids on the amino-silane-coated aluminum substrate, and (b) a digital photo of the corresponding liquids on the same sample.

The self-cleaning ability was tested using dirt on the amino-silane-modified sample, as shown in Figure 5. The water droplets (25 µL), placed on the sample inclined at 30°, roll down the superhydrophobic surface carrying dirt and other debris, leaving a clean sample. The full video can be seen in the supplementary data.

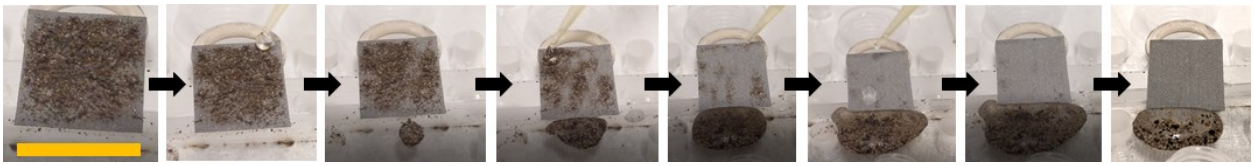

Figure 5. The self-cleaning test with water droplets rolling off an amino-silane-coated sample covered in dirt. The scale bar and all samples are 1 cm in size.

Switchable Evaporation Kinetics

Evaporation tests on various samples were conducted using single and two-droplet experiments. Single droplet experiments involved evaporating water or acetic acid droplets on different surfaces in the closed environmental chamber (Figure 1). The two-droplet experiments involved placing a droplet of water on the surface, followed by a second droplet of either water or acetic acid within 400 s of placing the first drop. The single droplet experiments show how surface wettability affects

evaporation kinetics through the lifetime of the droplet. The two-droplet experiments demonstrate how conventional non-wetting surfaces maintain relatively slow evaporation kinetics, while acetic acid on amino-silane-coated samples allows switching the wettability from non-wetting to wetting states on demand, which accelerates the evaporation process.

Figure 6(a) and (b) show the droplet volume and heater temperature versus time for a single water droplet deposited on an amino-silane-coated aluminum substrate. Figure 6(c) shows the evaporation rate calculated using Eqn. (2) and the slope of volume versus time data from the goniometer. The evaporation rate calculated using the volume data is relatively noisy compared to that of the temperature sensor, as evident in Figure 6(c). Moreover, resolving the droplet shape on superwetting surfaces and towards the end of its lifetime is challenging and error-prone. In this case, the uncertainty in temperature measurements and the corresponding calculated evaporation rates, denoted by shaded regions in Figures 6(b) and (c), are ± 0.5 ℃ and 0.005 µL/s, respectively. Figure 6(c) shows that the evaporation rates calculated using the goniometer are within the uncertainty bounds of the rates calculated using the heater's temperature sensor.

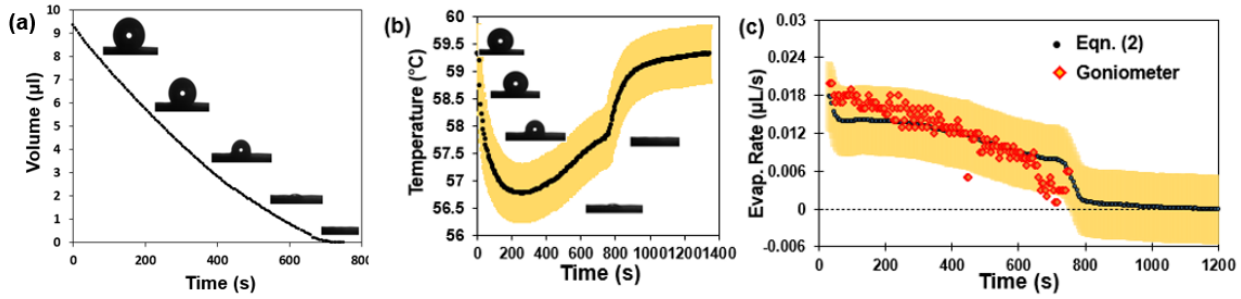

Figure 6. The temporal change in (a) heater temperature and (b) droplet volume when water evaporates on an amino-silane-coated sample. (c) Evaporation rates versus time calculated using Eqn. (2) and goniometer's volume data. The shaded region indicates the uncertainty in plotted parameter.

Figure 6(a) from the goniometer shows that for a 10 µL droplet, it takes approximately 780 seconds for complete evaporation, corresponding to an average rate of 0.0128 μL/s that agrees well with the results shown in Figure 6(c). The temperature change with time indicates a steep initial decrease since the evaporation rate and heat loss exceed the heating power. The temperature decreases until the heating power matches the evaporation rate and the heat loss. Beyond this stage, the temperature continuously increases until it reaches the initial state, where the heat loss balances the heat generation rate in the absence of the droplet. An inflection in the temperature rise occurs when the droplet evaporation is complete.

We compared the evaporation of water and acetic acid droplets on substrates coated with different molecules (Figure 7). Substrates coated with amino silane offer a unique opportunity to control evaporation kinetics. The evaporation rate of 10 µL-water drops is similar across all the non-wetting substrates coated with amino-silane, lauric acid, and FDTS (Figure 7(a-c)). With an initial evaporation rate close to 0.02 µL/s, the droplets take close to 900 s to evaporate completely. In this regard, even the evaporation of 10 µL droplets of acetic acid on lauric acid and FDTS-coated substrates is comparable to the evaporation of pure water. The change in slope observed near 700

s in all the experiments is due to a shift in evaporation characteristics. Around this time, the droplet-substrate contact area begins to decrease due to droplet recession, which results in a steeper drop in evaporation rate. A small yet repeatable anomaly is observed in the evaporation of acetic acid on lauric acid-coated samples (Figure 7(e)). Around 500 s, when the droplet becomes significantly smaller than the initial size (10 µL), it spreads on the surface, which increases the surface area for evaporation and the corresponding rate. A possible explanation is the wetting of regions not covered by lauric acid, which only occurs when the droplet becomes very small (less than the characteristic size of islands coated by lauric acid). This anomaly, unique to this liquid-substrate combination, is repeatable and also seen in two-drop experiments discussed later.

The evaporation of acetic acid on amino-silane (Figure 7(d)) is significantly different, with peak evaporation rates almost 3-times higher than those observed in other trials. In this case, we see peak evaporation rates close to 0.06 µL/s as opposed to peak values of 0.02 µL/s seen in other experiments. Figure 7(d) shows an initial steep increase, followed by steady evaporation and a steep decrease in the evaporation rate. The initial increase and the subsequent decrease in rate correspond to droplet spreading and receding on the surface, which changes the area available for evaporation. Unlike other trials, Figure 7(d) is different because acetic acid changes the wetting nature of the amino-silane-coated samples with a contact angle close to 0°.

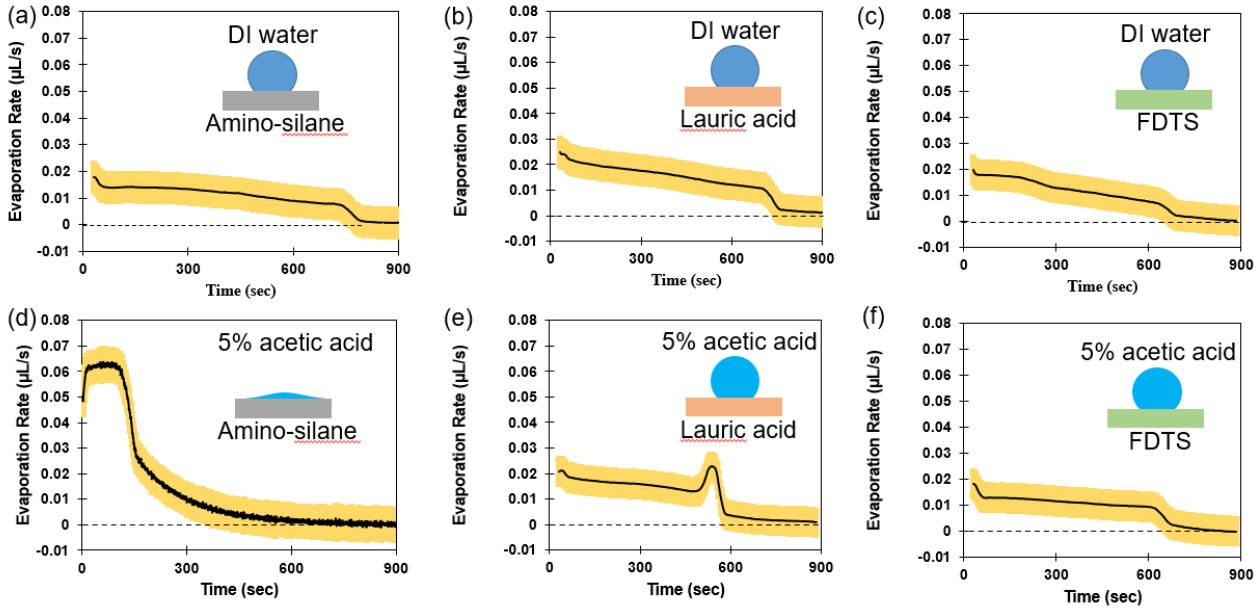

Figure 7. Evaporation rate in single-droplet experiments for (a) water on an amino-silane-coated sample, (b) water on a lauric acid-coated sample, (c) water on an FDTS-coated sample, (d) acetic acid on an amino-silane-coated sample, (e) acetic acid on a lauric acid-coated sample, (f) acetic acid on an FDTS-coated sample.

The change in surface wettability takes place due to changes in surface-attached amino-silane molecules in the presence of dilute acetic acid (Figure 8). The exposure of amino-silane to acetic acid results in amidation or the formation of amide, subsequently allowing hydrogen bonding with water. In effect, the polar interaction of water with the surface allows wetting, which is amplified

by the surface roughness. Amidation is easily reversible. In this case, dehydration or evaporation results in the removal of water and acetic acid, resulting in the recreation of the bond between the amine group and aluminum substrate, as illustrated below. Note that such a change in other surface functionalizing molecules (lauric acid and FDTS) does not occur with acetic acid because these molecules do not have the amine group that responds to the carboxylic group of the acetic acid. Hence, the evaporation kinetics remains fairly indifferent.

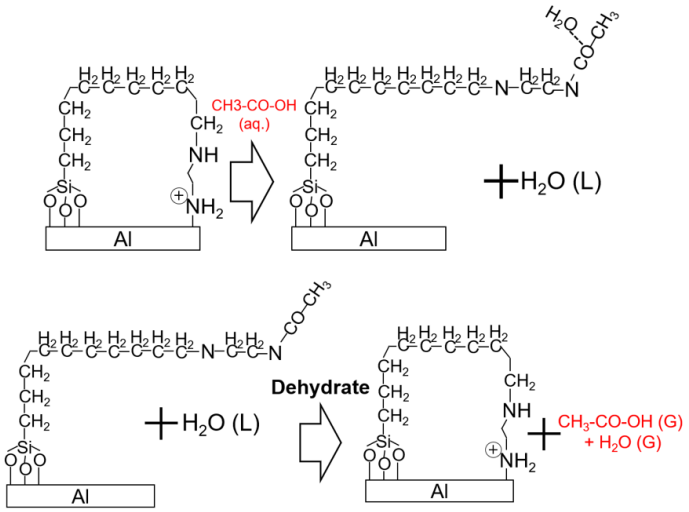

Figure 8. The mechanism governing the wettability of an amino-silane-coated surface

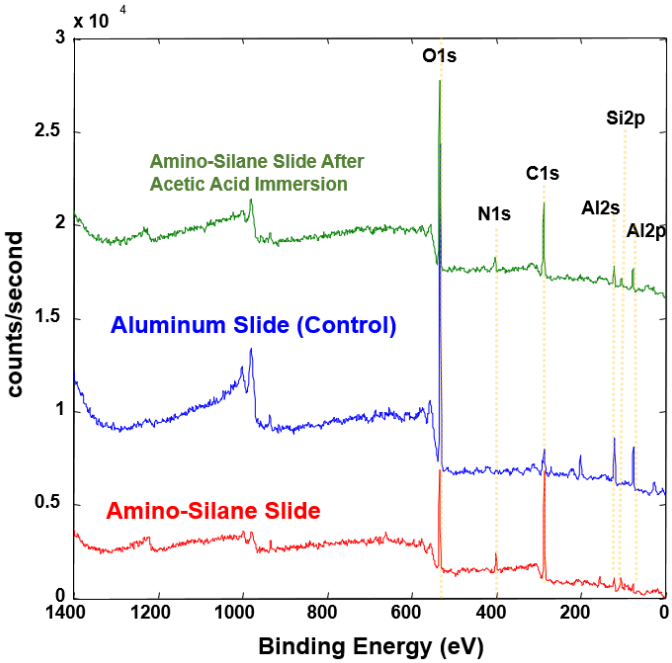

Figure 9. The XPS result of the bare aluminum slide, amino-silane coated slide and the amino-silane coated slide after being immersed in acetic acid.

XPS results provide further insight into the nature of amino-silane-coated samples before and after dipping in acetic acid (Figure 9). For comparison, a bare aluminum sample does not contain any

nitrogen and silicon peaks and has only a small amount of carbon from atmospheric contamination. The aluminum peaks are much more prominent since there is no silane coating. The functionalized sample contains nitrogen and silicon peaks from the amino-silane molecule and a significant increase in carbon atoms from the hydrocarbon backbone of the molecule. Even after exposure to acetic acid, nitrogen and silicon are still present on the surface, indicating that the coating has not been removed by acetic acid. However, the peaks corresponding to the nitrogen, carbon, and silicon atoms are diminished, indicating a decrease in the amount of amino-silane molecules on the surface. The first exposure to acetic acid is possibly removing excess amino-silane groups that are not covalently bonded to the aluminum surface, accounting for this difference in XRD. Losing the excess amino-silane molecules from the surface also decreases the contact angle after the first exposure to acetic acid, as noted in the surface durability tests (Figure 14).

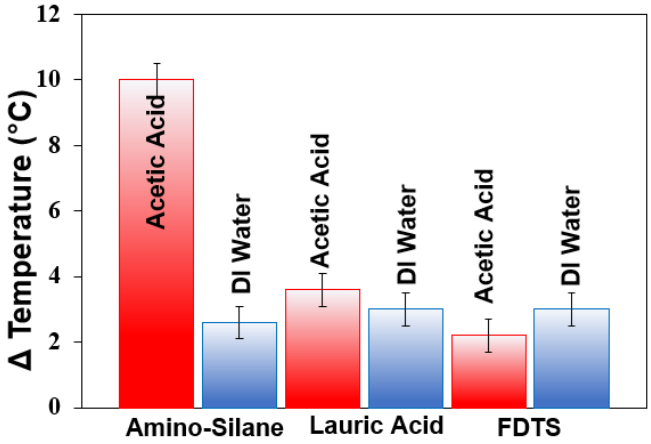

Figure 10. The peak temperature decrease during the evaporation of a single droplet of water or acetic acid on samples coated with amino-silane, lauric acid, and FDTS.

A sudden change in wettability has significant consequences on the self-cooling of surfaces during evaporation (Figure 10). With samples on the ceramic heater generating a constant heating power, evaporating DI-water drops have similar cooling effects. All samples show a close to 4 ºC peak temperature decrease due to evaporative cooling. In fact, even acetic acid drops on lauric acid-coated and FDTS-coated samples show a similar 4 ºC peak temperature drop. Evaporation of acetic acid on amino-silane-coated results in thin-film evaporation, which causes more than 14 ºC peak temperature drop – a 3.5-times increase compared to other trials.

The same experimental setup was used for two-droplet evaporation trials (Figure 1). In these tests, a water droplet was first placed on a surface-modified aluminum foil, followed by a second droplet of water or acetic acid to continue evaporation. Evaporation characteristics of water followed by another water droplet were similar on all non-wetting surfaces made using amino-silane, lauric acid, and FDTS. Evaporation of water followed by acetic acid droplets on lauric acid and FDTS-coated surfaces is also comparable to the other experiments. However, the evaporation characteristics of a water droplet followed by acetic acid on amino-silane are markedly different. This difference is due to the sudden modification in surface wettability, which results in significantly different cooling or temperature drop. This test demonstrated how wettability and evaporation kinetics could be controlled on demand.

Figure 11 compares the heater temperature in the two-droplet experiments on an amino-silane-coated aluminum substrate. Insets in Figure 11 show droplet shapes at crucial instances during the experiment. For an experiment involving two successive water drops, the evaporation characteristics and sample temperature do not change appreciably during the experiment. The peak temperature decrease is close to 4 °C, which occurs when the second droplet is added to a partially evaporated first drop. However, when an acetic acid droplet is introduced midway through the evaporation of the first water drop, wettability changes drastically. This change substantially improves liquid spreading across the substrate, resulting in thin-film evaporation that decreases the substrate temperature by more than 14 °C at peak cooling. The higher evaporation rates also result in a shorter experiment where 20 µL of working fluid (water + acetic acid) evaporates much quicker than two successive water drops. Specifically, to evaporate 95% of the total volume in a two-drop experiment using only DI water droplets takes 1035 s, whereas it is 605 s for a DI water droplet followed by a 5% acetic acid droplet.

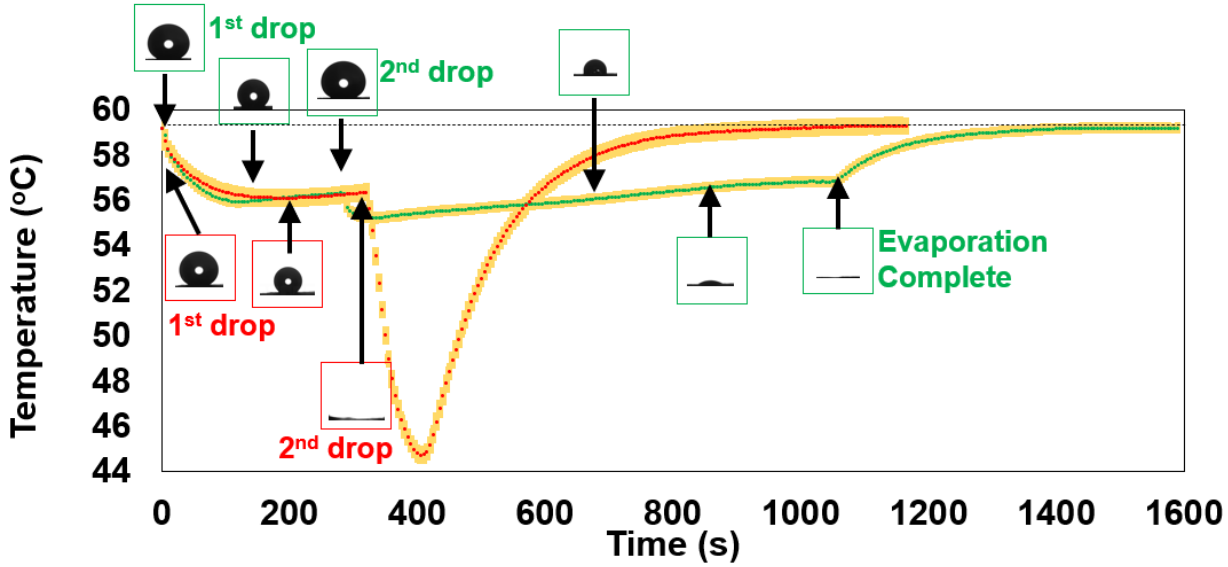

Figure 11. Temperature change during evaporation on an amino-silane-coated sample when a water droplet is added to a water droplet versus an acetic acid droplet added to a water droplet.

We now compare evaporation rates in two-droplet experiments to show that the change in cooling characteristics only occurs when acetic acid is used on an amino-silane-coated substrate. The evaporation rate for all six combinations of working fluids and substrate coatings is shown in Figure 12. Generally, for two successive water drops on amino-silane, lauric acid, and FDTS-coated substrates (Figure 12a-c), there is a gradual decrease in evaporation rate followed by a spike and then a decrease again. A sudden decline in rate is seen at the final stages of evaporation, which also occurs in single droplet experiments. This decline corresponds to the disappearance of tiny droplets. On the contrary, thin-film evaporation is efficient from the very beginning. Hence, a sudden drop in the rate is not seen in acetic acid wetting amino-silane-coated samples (Figure 7d, Figure 12d) – it is a gradual approach to complete evaporation. Even in these experiments, the anomaly associated with acetic acid as the second droplet on lauric acid-coated substrates is seen near the end of evaporation at around 900 s (Figure 12e) with a spike in evaporation rate due to

reasons explained earlier. These experiments show that acetic acid can significantly improve the evaporation rate of water on amino-silane when necessary. Peak evaporation rates in most experiments correspond to 0.03-0.04 µL/s, whereas water followed by 5% acetic acid droplets correspond to a peak rate exceeding 0.12 µL/s. When lower rates are sufficient, non-wetting droplets can provide a nominally low uniform evaporation rate, but adding acetic acid will enhance the average evaporation rate by 3-times.

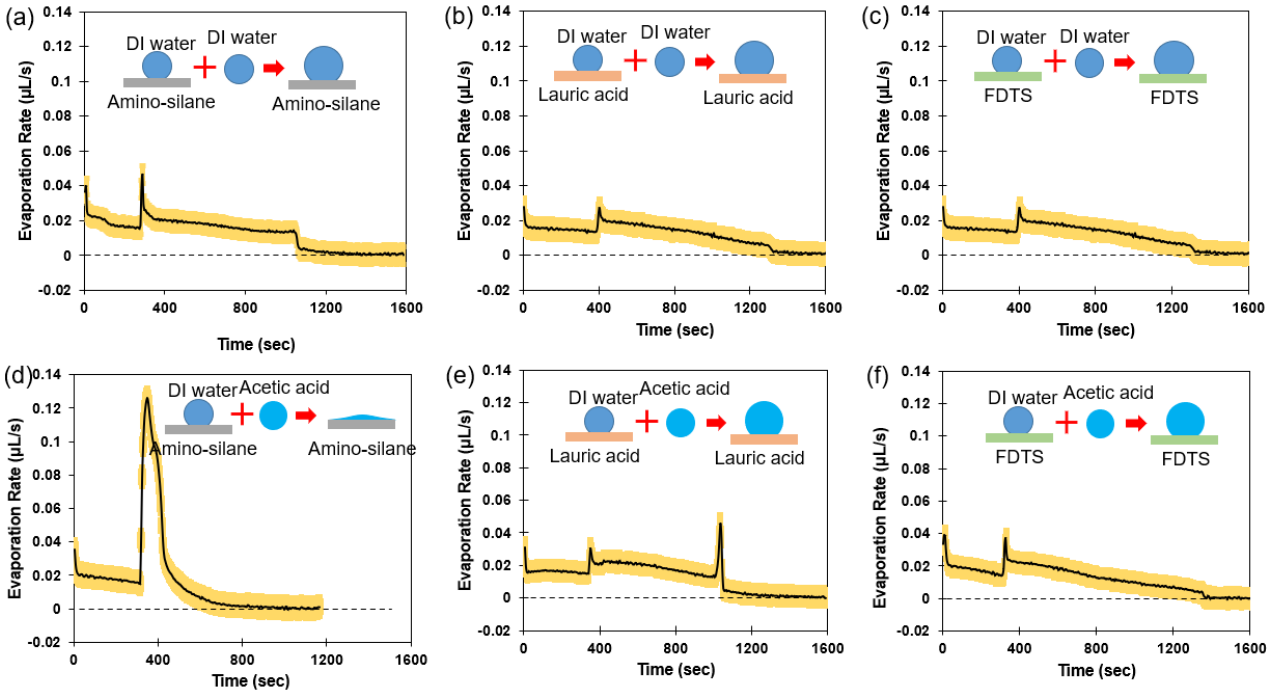

Figure 12. Two-droplet evaporation tests consist of adding a second drop after partial evaporation of the first drop. The top row shows the evaporation rate of two successive water droplets on (a) amino-silane, (b) lauric acid, and (c) FDTS-coated substrate. The bottom row shows the evaporation rate of water followed by an acetic acid droplet on (d) amino-silane, (e) lauric acid, and (f) FDTS-coated substrate.

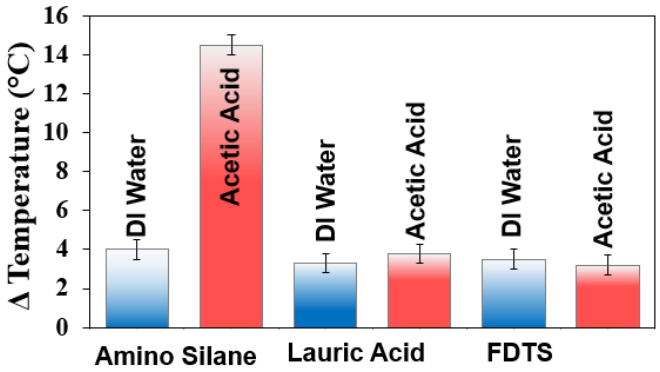

Figure 13. The peak temperature change with the addition of either water or acetic acid droplets

Figure 13 compares the cooling or peak temperature decrease in the two-droplet experiments across different trials. While cooling is close to 4 °C in most experiments, it is more than 3-times

higher (>14 °C) when acetic acid is used on the amino-silane-coated substrate. The acetic acid droplets on lauric acid and the FDTS-modified samples do not have an enhanced cooling effect since the surface wettabilities do not change with the addition of acetic acid.

Repeatability

The wettability switching mechanism was tested multiple times to ensure repeatability. The testing cycle consisted of measuring the contact angle with water, then measuring the contact angle with an acetic acid droplet, then rinsing with water droplets allowing for complete evaporation, and then measuring the contact angle with water again. Twenty cycles of this test are shown in Figure 14. The acetic acid droplet always showed complete wetting with a contact angle of ~ 0°. Similarly, the water droplet always shows contact angles exceeding 145°. After the first cycle, the water contact angle decreased from 153° to 145°; however, subsequent measurements showed similar contact angles. The chemical stability of the surface in acetic acid solutions of various concentrations is discussed in the supplementary information.

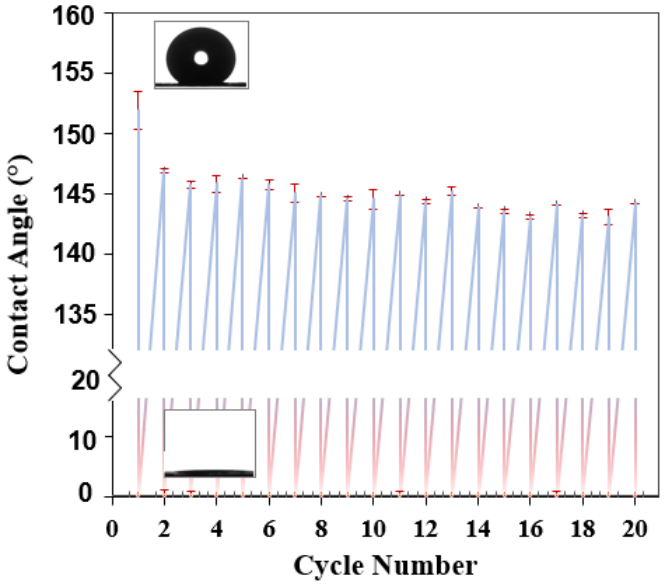

Figure 14. The contact angle measured after each cycle of immersing the amino-silane sample in water and acetic acid followed by complete evaporation.

The enhancement of evaporative cooling of a surface can lead to new and promising ways of lowering the temperature of electrical components or entire power systems. With switchable wettability, a self-cleaning superhydrophobic surface can dynamically change to a superhydrophilic surface with high heat transfer rates due to the formation of thin films. Our results also show that the surface can maintain its chemical composition after several cycles of reversible switching and interaction of liquids from everyday use.

Conclusions

This study demonstrates a self-cleaning superhydrophobic aluminum surface that can dynamically switch its wettability to yield a superhydrophilic surface advantageous for evaporative cooling

using water. The surface becomes superhydrophobic again after complete evaporation. This reversible behavior of switching between equilibrium contact angles of 145° and 0° is due to the amino-silane-functionalized surface that changes wetting characteristics when exposed to acetic acid. Similar behavior is not seen in typical non-wetting coatings like lauric acid and perfluorodecyltrichlorosilane (FDTS) since they lack the amine group. In the non-wetting state, surfaces made with amino-silane, lauric acid, and FDTS all show similar evaporation behavior. Specifically, evaporation of a 10 μL water droplet takes place at 0.02 μL/s resulting in a surface temperature decrease of 4 ℃ ± 0.5 ℃. On the other hand, evaporation of 5% acetic acid (v/v) (10 μL droplet) on an amino-silane-coated surface takes place at 0.06 μL/s yielding a surface temperature decrease of 14 ℃. Such switching over wetting and evaporation behavior can be instrumental in several applications, including nanoscale fabrication, inkjet printing, and self-cleaning electronics.

Acknowledgments

This work was sponsored by the American Chemical Society's Petroleum Research Fund Doctoral New Investigator Grant. Acknowledgment is made to the Donors of the American Chemical Society Petroleum Research Fund for support of this research. S. Narayan also acknowledges the support from the National Science Foundation's Division of Chemical, Bioengineering, Environmental, and Transport Systems in the Directorate for Engineering under Grant No. 1944323.

Supplementary Data

Please see the uploaded videos, data and theoretical analysis (e-component).

References

(1) Gogolides, E.; Ellinas, K.; Tserepi, A. Hierarchical Micro and Nano Structured, Hydrophilic, Superhydrophobic and Superoleophobic Surfaces Incorporated in Microfluidics, Microarrays and Lab on Chip Microsystems. *Microelectron. Eng.* **2015**, *132*, 135–155. https://doi.org/10.1016/j.mee.2014.10.002.

(2) Lim, J. A.; Lee, W. H.; Kwak, D.; Cho, K. Evaporation-Induced Self-Organization of Inkjet-Printed Organic Semiconductors on Surface-Modified Dielectrics for High-Performance Organic Transistors. *Langmuir* **2009**, *25* (9), 5404–5410. https://doi.org/10.1021/la804269q.

(3) Ma, Y.; Kaczynski, J.; Ranacher, C.; Roshanghias, A.; Zauner, M.; Abasahl, B. Nano-Porous Aluminum Oxide Membrane as Filtration Interface for Optical Gas Sensor Packaging. *Microelectron. Eng.* **2018**, *198* (June), 29–34. https://doi.org/10.1016/j.mee.2018.06.013.

(4) Calvert, P. Inkjet Printing for Materials and Devices. **2001**, 3299–3305.

(5) Golichenari, B.; Nosrati, R.; Farokhi-fard, A.; Faal, M. Electrochemical-Based Biosensors for Detection of Mycobacterium Tuberculosis and Tuberculosis Biomarkers. **2019**, *39* (8), 1056–1077.

(6) Belmiloud, N.; State, J. S.; Technol, S.; Belmiloud, N.; Tamaddon, A. H.; Mertens, P. W.;

Struyf, H.; Xu, X. Science and Technology Dynamics of the Drying Defects Left by Residual Ultra-Pure Water Droplets on Silicon Substrate Dynamics of the Drying Defects Left by Residual Ultra-Pure Water. **2012**. https://doi.org/10.1149/2.014201jss.

(7) Wemp, C. K.; Carey, V. P. Tuning Superhydrophilic Nanostructured Surfaces to Maximize Water Droplet Evaporation Heat Transfer Performance. *J. Heat Transfer* **2018**, *140* (10), 1–10. https://doi.org/10.1115/1.4040142.

(8) Zhang, G.; Xu, Y.; Duan, Z.; Li, L.; Liu, C.; Yao, W. Applied Surface Science Enhancement of Evaporative Heat Transfer on Carbon Nanotube Sponges by Electric Fi Eld Reinforced Wettability. *Appl. Surf. Sci.* **2018**, *454* (April), 262–269. https://doi.org/10.1016/j.apsusc.2018.05.110.

(9) Günay, A. A.; Gnadt, M.; Sett, S.; Vahabi, H.; Kota, A. K.; Miljkovic, N. Droplet Evaporation Dynamics of Low Surface Tension Fluids Using the Steady Method. *Langmuir* **2020**, *36* (46), 13860–13871. https://doi.org/10.1021/acs.langmuir.0c02272.

(10) Pan, Z.; Weibel, J. A.; Garimella, S. V. International Journal of Heat and Mass Transfer Transport Mechanisms during Water Droplet Evaporation on Heated Substrates of Different Wettability. *Int. J. Heat Mass Transf.* **2020**, *152*, 119524. https://doi.org/10.1016/j.ijheatmasstransfer.2020.119524.

(11) Kadhim, M. A.; Kapur, N.; Summers, J. L.; Thompson, H. Experimental and Theoretical Investigation of Droplet Evaporation on Heated Hydrophilic and Hydrophobic Surfaces. *Langmuir* **2019**, *35* (19), 6256–6266. https://doi.org/10.1021/acs.langmuir.8b03601.

(12) Gibbons, M. J.; Di Marco, P.; Robinson, A. J. Heat Flux Distribution beneath Evaporating Hydrophilic and Superhydrophobic Droplets. *Int. J. Heat Mass Transf.* **2020**, *148*, 119093. https://doi.org/10.1016/j.ijheatmasstransfer.2019.119093.

(13) Cheng, H.; Jiang, Z.; Chang, T.; Chen, P. Effects of Difference in Wettability Level of Biphilic Patterns on Copper Tubes in Pool Boiling Heat Transfer. *Exp. Therm. Fluid Sci.* **2021**, *120* (August 2020), 110241. https://doi.org/10.1016/j.expthermflusci.2020.110241.

(14) Zhong, X.; Ren, J.; Duan, F. Wettability Effect on Evaporation Dynamics and Crystalline Patterns of Sessile Saline Droplets. *J. Phys. Chem. B* **2017**, *121* (33), 7924–7933. https://doi.org/10.1021/acs.jpcb.7b03690.

(15) Lee, S.; Kim, D. I.; Kim, Y. Y.; Park, S. E.; Choi, G.; Kim, Y.; Kim, H. J. Droplet Evaporation Characteristics on Transparent Heaters with Different Wettabilities. *RSC Adv.* **2017**, *7* (72), 45274–45279. https://doi.org/10.1039/c7ra08888d.

(16) Wang, X.; Hsieh, M.-L.; Bur, J. A.; Lin, S.-Y.; Narayanan, S. Capillary-Driven Solar-Thermal Water Desalination Using a Porous Selective Absorber. *Mater. Today Energy* **2020**, *17*, 100453. https://doi.org/10.1016/j.mtener.2020.100453.

(17) Murray, B.; Fox, M. J.; Narayan, S. Analyzing Interfacial Transport for Water Evaporating into Dry Nitrogen. *Appl. Therm. Eng.* **2022**, *202* (August 2021), 117910. https://doi.org/10.1016/j.applthermaleng.2021.117910.

(18) Perkins-Howard, B.; Walker, A. R.; Do, Q.; Senadheera, D. I.; Hazzazi, F.; Grundhoefer, J. P.; Daniels-Race, T.; Garno, J. C. Surface Wettability Drives the Crystalline Surface Assembly of Monodisperse Spheres in Evaporative Colloidal Lithography. *J. Phys. Chem.*

C **2022**, *126* (1), 505–516. https://doi.org/10.1021/acs.jpcc.1c07098.

(19) Hartmann, M.; Hardt, S. Stability of Evaporating Droplets on Chemically Patterned Surfaces. *Langmuir* **2019**, *35* (14), 4868–4875. https://doi.org/10.1021/acs.langmuir.9b00172.

(20) Dai, C.; Liu, N.; Cao, Y.; Chen, Y.; Lu, F.; Feng, L. Fast Formation of Superhydrophobic Octadecylphosphonic Acid (ODPA) Coating for Self-Cleaning and Oil/Water Separation. *Soft Matter* **2014**, *10* (40), 8116–8121. https://doi.org/10.1039/c4sm01616e.

(21) Xiong, J.; Das, S. N.; Kar, J. P.; Choi, J. H.; Myoung, J. M. A Multifunctional Nanoporous Layer Created on Glass through a Simple Alkali Corrosion Process. *J. Mater. Chem.* **2010**, *20* (45), 10246–10252. https://doi.org/10.1039/c0jm01695k.

(22) Vazirinasab, E.; Maghsoudi, K.; Jafari, R.; Momen, G. A Comparative Study of the Icephobic and Self-Cleaning Properties of Teflon Materials Having Different Surface Morphologies. *J. Mater. Process. Technol.* **2020**, *276* (June 2019), 116415. https://doi.org/10.1016/j.jmatprotec.2019.116415.

(23) Bi, Y.; Wang, Z.; Lu, L.; Niu, X.; Gu, Y.; Wang, L. Progress in Organic Coatings A Facile Route to Engineer Highly Superhydrophobic Antibacterial Fi Lm through Polymerizable Emulsi Fi Er. **2019**, *133* (February), 387–394. https://doi.org/10.1016/j.porgcoat.2019.04.071.

(24) Agrawal, N.; Si, J.; Tan, J.; Low, P. S.; Wen, E.; Fong, M.; Lai, Y.; Chen, Z. Green Synthesis of Robust Superhydrophobic Antibacterial and UV-Blocking Cotton Fabrics by a Dual-Stage Silanization Approach. **2019**, *1900032*, 1–10. https://doi.org/10.1002/admi.201900032.

(25) Yang, Y.; Cui, G.; Lan, C. Q. Developments in Evaporative Cooling and Enhanced Evaporative Cooling - A Review. *Renew. Sustain. Energy Rev.* **2019**, *113* (June), 109230. https://doi.org/10.1016/j.rser.2019.06.037.

(26) Lee, M.; Kim, W.; Lee, S.; Baek, S.; Yong, K.; Jeon, S. Water Droplet Evaporation from Sticky Superhydrophobic Surfaces. *Appl. Phys. Lett.* **2017**, *111* (2). https://doi.org/10.1063/1.4992140.

(27) Dash, S.; Garimella, S. V. Droplet Evaporation Dynamics on a Superhydrophobic Surface with Negligible Hysteresis. *Langmuir* **2013**, *29* (34), 10785–10795. https://doi.org/10.1021/la402784c.

(28) Mahmud, M. A.; MacDonald, B. D. Experimental Investigation of Interfacial Energy Transport in an Evaporating Sessile Droplet for Evaporative Cooling Applications. *Phys. Rev. E* **2017**, *95* (1), 1–8. https://doi.org/10.1103/PhysRevE.95.012609.

(29) Pati, A. R.; Panda, A.; Lily; Munshi, B.; Kumar, A.; Sahoo, A.; Ghosh, S.; Mohapatra, S. S. Dropwise Evaporative Cooling of Hot Water: A Novel Methodology to Enhance Heat Transfer Rate at Very High Surface Temperatures. *Int. J. Therm. Sci.* **2018**, *127* (January), 335–350. https://doi.org/10.1016/j.ijthermalsci.2018.01.028.

(30) Romashevskiy, S. A.; Ovchinnikov, A. V. Functional Surfaces with Enhanced Heat Transfer for Spray Cooling Technology. *High Temp.* **2018**, *56* (2), 255–262. https://doi.org/10.1134/S0018151X18020244.

(31) Abada, D.; Maalouf, C.; Sotehi, O.; Rouag-Saffidine, D.; Polidori, G.; Boudjabi, A. F.; Derghout, Z. Performance Evaluation of Fabrics for Evaporative Cooling Applications. *Energy Build.* **2022**, *266*, 112120. https://doi.org/10.1016/j.enbuild.2022.112120.

(32) Wang, J. N.; Liu, Y. Q.; Zhang, Y. L.; Feng, J.; Wang, H.; Yu, Y. H.; Sun, H. B. Wearable Superhydrophobic Elastomer Skin with Switchable Wettability. *Adv. Funct. Mater.* **2018**, *28* (23), 1–8. https://doi.org/10.1002/adfm.201800625.

(33) Verplanck, N.; Coffinier, Y.; Thomy, V.; Boukherroub, R. Wettability Switching Techniques on Superhydrophobic Surfaces. *Nanoscale Res. Lett.* **2007**, *2* (12), 577–596. https://doi.org/10.1007/s11671-007-9102-4.

(34) Su, M. J.; Bai, S.; Luo, Y.; Chu, G. W.; Sun, B. C.; Le, Y.; Chen, J. F. Controllable Wettability on Stainless Steel Substrates with Highly Stable Coatings. *Chem. Eng. Sci.* **2019**, *195*, 791–800. https://doi.org/10.1016/j.ces.2018.10.025.

(35) Namaee-Ghasemi, A.; Behbahani, H. S. zadeh; Kord, S.; Sharifi, A. Simulation and Analysis of Dynamic Wettability Alteration and Correlation of Wettability-Related Parameters during Smart Water Injection in a Carbonate Core. *J. Mol. Liq.* **2021**, *331*. https://doi.org/10.1016/j.molliq.2021.115741.

(36) Pourjavadi, A.; Kohestanian, M.; Streb, C. Materials Science & Engineering C PH and Thermal Dual-Responsive Poly (NIPAM- Co -GMA) -Coated Magnetic Nanoparticles via Surface-Initiated RAFT Polymerization for Controlled Drug Delivery. *Mater. Sci. Eng. C* **2020**, *108* (October 2019), 110418. https://doi.org/10.1016/j.msec.2019.110418.

(37) Parisi, G.; Narayan, S. Journal of Water Process Engineering Using a Fluorine-Free Copper Mesh with Dynamically Tunable Wetting Properties for High-Flux Separation of Oil-Water Mixtures. *J. Water Process Eng.* **2021**, *44* (October), 102365. https://doi.org/10.1016/j.jwpe.2021.102365.

(38) Zhang, L.; Deng, X.; Hu, H.; Chen, B.; Cheng, G.; Gao, G. Superhydrophilic Al2O3 Composite Meshes for Continuous High-Efficiency Oil-Water Separation. *Mater. Lett.* **2020**, *274*, 127892. https://doi.org/10.1016/j.matlet.2020.127892.

(39) Wang, X.; Wang, X.; Liu, Y.; Liu, Y.; Zhang, M.; Zhang, M.; Luo, Z.; Luo, Z.; Yang, D.; Yang, D. Beadlike Porous Fibrous Membrane with Switchable Wettability for Efficient Oil/Water Separation. *Ind. Eng. Chem. Res.* **2020**, *59* (23), 10894–10903. https://doi.org/10.1021/acs.iecr.0c01103.

(40) Ludwicki, J. M.; Robinson, F. L.; Steen, P. H. Switchable Wettability for Condensation Heat Transfer. *ACS Appl. Mater. Interfaces* **2020**, *12* (19), 22115–22119. https://doi.org/10.1021/acsami.0c01523.

(41) Watlow. *ULTRAMIC® Advanced Ceramic Heaters*. https://www.watlow.com/products/heaters/specialty-heaters/ultramic-ceramic-heaters (accessed 2022-11-10).

(42) T-GlobalTechnology. *S606C/TG-AS606C Thermal Grease*. https://www.tglobalcorp.com/s606c-thermal-grease (accessed 2022-11-10).

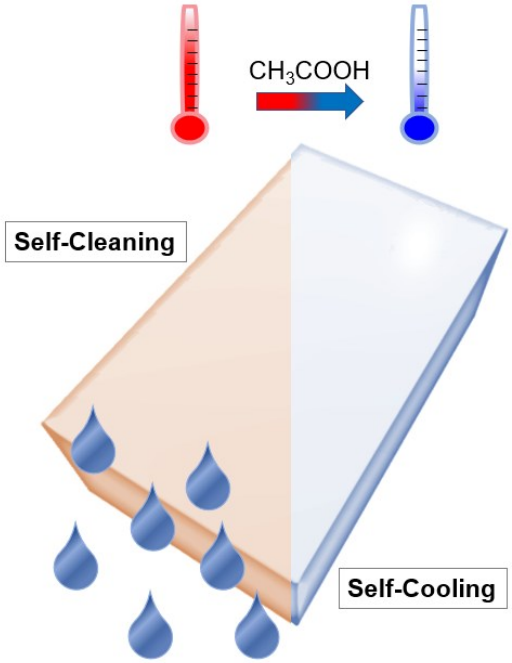
CH3COOH
Self-Cleaning
Self-Cooling

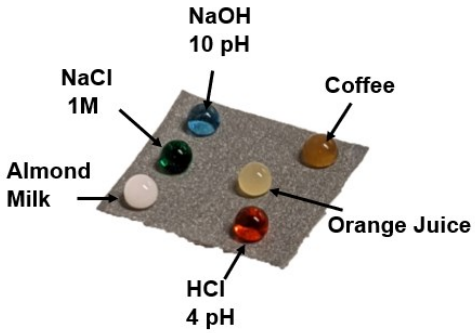
NaOH
10 pH
NaCl
1M
Coffee
Almond
Milk
Orange Juice
HCl
4 pH

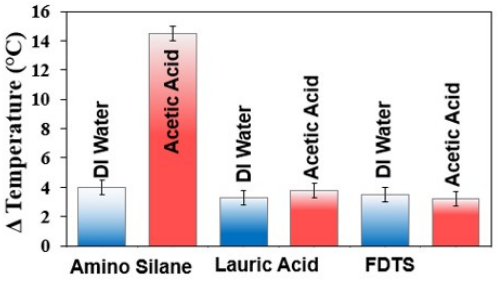
Δ Temperature (°C)
16
14
12
10
8
6
4
2
0
DI Water
Acetic Acid
DI Water
Acetic Acid
DI Water
Acetic Acid
Amino Silane
Lauric Acid
FDTS